Audio Engineering Society

Convention Paper

Presented at the 138th Convention
2015 May 7–10 Warsaw, Poland

Sound Field Synthesis of Virtual Cylindrical Waves using Circular and Spherical Loudspeaker Arrays

Nara Hahn and Sascha Spors

Institute of Communications Engineering, University of Rostock, Rostock, Germany

Correspondence should be addressed to Nara Hahn (nara.hahn@uni-rostock.de)

ABSTRACT

In sound field synthesis, like near-field compensated higher-order Ambisonics or Wave Field Synthesis, various virtual source models are used to describe a virtual sound scene. In near-field compensated higher-order Ambisonics, the virtual sound field has to be expanded into spherical harmonics. Unlike plane waves and spherical waves, cylindrical waves are not conveniently represented in the spherical harmonics domain. In this paper, we tackle this problem and derive closed form driving functions for virtual cylindrical waves. The physical properties of synthesized sound fields are investigated through numerical simulations, where the results are compared with virtual cylindrical waves in wave field synthesis.

1. INTRODUCTION

Sound field synthesis is a spatial sound reproduction approach, the aim of which is the physical reconstruction of a desired sound field within a listening area, using a dense distribution of secondary sources. The secondary sources are realized by loudspeakers that are driven by individual driving functions. Well-known analytic sound field synthesis methods are Wave Field Synthesis (WFS), near-field compensated higher-order Ambisonics (NFC-HOA), and the spectral division method (SDM) [1, 2, 3, 4].

The desired sound field can be obtained either by a spatial recording in combination with sound field analysis, or by physical model describing a virtual sound field. The former approach is termed as *data-based* representation, and the latter as *model-based* representation. In model-based sound field synthesis, various virtual source models are employed. While virtual plane waves and spherical waves are frequently used, cylindrical wave models seem to have gained less attention. This is probably because (i) a spherical harmonics representation is not known, (ii) it involves Hankel functions who are computationally complex to implement, whereas (iii) point sources can be implemented efficiently and thus are preferred in modeling radially propagating

waves. To the authors knowledge, the NFC-HOA driving function of a virtual cylindrical wave has not been published so far, whereas the corresponding WFS and SDM driving functions are known [4, 5].

In [6, Sec. 5.3.4], it was noted that the amplitude of virtual spherical waves seems to attenuate much faster than one might expect from a real source. Although the auditory distance perception in sound field synthesis is still an open topic, a virtual line source could be an alternative to achieve a mild amplitude decay.

This paper derives the NFC-HOA driving function for virtual cylindrical waves in closed form. First, we formulate the relation between the circular and spherical harmonics representation, under the assumption that the sound field is independent to the vertical axis (Sec. 2). Circular harmonics expansion coefficients are converted to spherical expansion coefficients, which are then plugged into the general NFC-HOA driving function (Sec. 3). The reproduced sound fields are numerically simulated, and the physical properties are examined with special attention to the amplitude decay (Sec. 4).

1.1. Nomenclature

A sound field in the frequency domain is denoted by uppercase $S(\mathbf{x}, \omega)$, and a vector like e.g. position $\mathbf{x}$ by lowercase boldface. The radial frequency ω is related to the temporal frequency $\omega = 2\pi f$. For monochromatic plane waves, we use the convention $e^{-i\mathbf{k}_{\text{pw}}^T\mathbf{x}}$, where the direction of $\mathbf{k}_{\text{pw}}$ indicates the propagation direction and its norm the wavenumber, $k = \|\mathbf{k}_{\text{pw}}\|$ which satisfies the dispersion relation $k = \frac{2\pi f}{c}$ with c being the speed of sound. The time dependent phase $e^{i\omega t}$ is omitted. Cylindrical coordinate representation (ρ, ϕ, z) is related to the Cartesian coordinates (x, y, z) by

$$\begin{aligned} x &= \rho\cos\phi \\ y &= \rho\sin\phi \\ z &= z \end{aligned}$$

where ρ is the distance from the z-axis and ϕ the polar angle. The spherical coordinate representation (r, α, β) is related to the Cartesian representation by

$$\begin{aligned} x &= r\cos\alpha\sin\beta \\ y &= r\sin\alpha\sin\beta \\ z &= r\cos\beta, \end{aligned}$$

where r is the distance from the origin, α the azimuth angle, and β the colatitude angle. The complex unit i is defined as $i^2 = -1$. The subscripts 'pw', 'ls', and 'ps' are the abbreviations for plane wave, line source, and point source, respectively.

2. REPRESENTATION OF SOUND FIELDS

In the following, two-dimensional (2D) sound fields independent to one spatial coordinate are mainly considered. Without loss of generality, we assume that the vertical axis (z-axis or $\beta = 0$) is the invariant coordinate. For instance, an infinite-length cylindrical radiator with z-independent particle velocity emits a 2D sound field. It is further assumed that no sound source, sink, nor scatterer is in the evaluation region, i.e., only homogeneous regions are considered.

2.1. Circular Harmonics Representation

In cylindrical coordinates, a height-invariant 2D sound field $S(\rho, \phi, z, \omega) = S(\rho, \phi, \omega)$ can be expanded into circular harmonics $e^{im\phi}$,

$$S(\rho, \phi, \omega) = \sum_{m=-\infty}^{\infty} \mathring{S}_m(\omega) J_m\big(\tfrac{\omega}{c}\rho\big) e^{im\phi}, \qquad (1)$$

where $\mathring{S}_m(\omega)$ denotes the expansion coefficient, $J_m\big(\frac{\omega}{c}\rho\big)$ the m-th order Bessel function of the first kind. Equation (1) can be regarded as a Fourier series expansion with coefficients $\mathring{S}_m J_m\big(\frac{\omega}{c}\rho\big)$.

The circular harmonics expansion of a plane wave with $\mathbf{k}_{\text{pw}} = (k_x, k_y, 0)$ is [7, (2.41)]

$$e^{-i\mathbf{k}_{\text{pw}}^T\mathbf{x}} = \sum_{m=-\infty}^{\infty} i^{-m} J_m\big(\tfrac{\omega}{c}\rho\big) e^{im\phi}, \qquad (2)$$

and the expansion of a monopole line source at $\rho = \rho_{\text{ls}}$, $\phi = \phi_{\text{ls}}$ is [8, (8.53)]

$$\begin{aligned} &-\tfrac{i}{4} H_0^{(2)}\big(\tfrac{\omega}{c}\|\mathbf{x} - \mathbf{x}_{\text{ls}}\|\big) = \\ &= \sum_{m=-\infty}^{\infty} -\tfrac{i}{4} H_m^{(2)}\big(\tfrac{\omega}{c}\rho_{\text{ls}}\big) J_m\big(\tfrac{\omega}{c}\rho\big) e^{im(\phi-\phi_{\text{ls}})}. \end{aligned} \qquad (3)$$

for $\forall\rho < \rho_{\text{ls}}$. They are listed in Table 1. The expansion coefficients for higher order line sources can be obtained by exploiting the addition theorem of

source type	$\mathring{S}_m(\omega)$	$\breve{S}_n^m(\omega)$
plane wave	$i^{-m}e^{-im\phi_{\mathrm{pw}}}$	$4\pi i^{-n}Y_n^m(\beta_{\mathrm{pw}},\alpha_{\mathrm{pw}})^*$
line source	$-\frac{i}{4}H_m^{(2)}\big(\frac{\omega}{c}\rho_{\mathrm{ls}}\big)e^{-im\phi_{\mathrm{ls}}}$	$-\pi i^{m-n+1}H_m^{(2)}\big(\frac{\omega}{c}r_{\mathrm{ls}}\big)Y_n^m(\frac{\pi}{2},\alpha_{\mathrm{ls}})^*$
point source	—	$-i\frac{\omega}{c}h_n^{(2)}\big(\frac{\omega}{c}r_{\mathrm{ps}}\big)Y_n^m(\beta_{\mathrm{ps}},\alpha_{\mathrm{ps}})^*$

Table 1: Circular and spherical harmonics expansion coefficients for selected source types. Note that the coefficients for line source and point source are only valid in the interior region ($\rho < \rho_{\mathrm{ls}}$ and $r < r_{\mathrm{ls}}$). The spherical harmonic expansion coefficient of a monopole line source (colored cell) is derived in Sec. 2.3.

Bessel functions [9, (9.1.75)],

$$S(\mathbf{x},\omega) = \sum_{m=-\infty}^{\infty} J_m\big(\tfrac{\omega}{c}\rho\big)e^{im\phi}\times \times \underbrace{\sum_{\mu=-\infty}^{\infty} H_{\mu-m}^{(2)}\big(\tfrac{\omega}{c}\rho_{\mathrm{ls}}\big)J_\mu\big(\tfrac{\omega}{c}\rho\big)e^{i(m-\mu)\phi_{\mathrm{ls}}}e^{i\mu\phi}}_{\mathring{S}_m(\omega)}, \quad (4)$$

for $\forall\rho < \rho_{\mathrm{ls}}$.

2.2. Spherical Harmonics Representation

In spherical coordinates, a homogeneous 3D sound field can be represented by the spherical harmonics expansion,

$$S(r,\alpha,\beta,\omega) = \sum_{n=0}^{\infty}\sum_{m=-n}^{n} \breve{S}_n^m(\omega)j_n\big(\tfrac{\omega}{c}r\big)Y_n^m(\beta,\alpha) \quad (5)$$

where $\breve{S}_n^m(\omega)$ denotes the expansion coefficient, $j_n\big(\frac{\omega}{c}r\big)$ the spherical Bessel function, and $Y_n^m(\beta,\alpha)$ a spherical harmonic, defined as

$$Y_n^m(\beta,\alpha) = \sqrt{\tfrac{2n+1}{4\pi}\tfrac{(n-m)!}{(n+m)!}}P_n^m(\cos\beta)e^{im\alpha}, \quad (6)$$

with $P_n^m(\cos\beta)$ being the associated Legendre function. Note that,

$$Y_n^m(\beta,\alpha) = Y_n^m(\beta,0)e^{im\alpha} \quad (7)$$

$$Y_n^m(\beta,\alpha)^* = Y_n^m(\beta,0)e^{-im\alpha}. \quad (8)$$

A plane wave propagating parallel to the xy-plane, $\beta_{\mathrm{pw}} = \frac{\pi}{2}$, is expanded as [7, (2.32)]

$$e^{-i\mathbf{k}_{\mathrm{pw}}^T\mathbf{x}} = \sum_{n=0}^{\infty}\sum_{m=-n}^{n} 4\pi i^{-n}j_n\big(\tfrac{\omega}{c}r\big)\times \times Y_n^m(\tfrac{\pi}{2},\alpha_{\mathrm{pw}})^*Y_n^m(\beta,\alpha), \quad (9)$$

and a point source at $\mathbf{x}_{\mathrm{ps}} = (r_{\mathrm{ps}},\alpha_{\mathrm{ps}},\beta_{\mathrm{ps}})$ as [8, (8.22)]

$$\frac{1}{4\pi}\frac{e^{-i\frac{\omega}{c}\|\mathbf{x}-\mathbf{x}_{\mathrm{ps}}\|}}{\|\mathbf{x}-\mathbf{x}_{\mathrm{ps}}\|} = \sum_{n=0}^{\infty}\sum_{m=-n}^{n} -i\tfrac{\omega}{c}h_n^{(2)}\big(\tfrac{\omega}{c}r_{\mathrm{ps}}\big)\times \times j_n\big(\tfrac{\omega}{c}r\big)Y_n^m(\beta_{\mathrm{ps}},\alpha_{\mathrm{ps}})^*Y_n^m(\beta,\alpha), \quad (10)$$

also listed in Table 1. Although the latter is not a 2D sound field, it was included as practical sound field synthesis systems employ secondary point sources. Unlike in Sec. 2.1, a 2D sound field is not straightforwardly degenerated in the spherical harmonics representation.

2.3. Converting $\mathring{S}_m(\omega)$ to $\breve{S}_n^m(\omega)$

In order to reveal the relation of circular and spherical harmonics expansion coefficients in a 2D sound field, (5) is reformulated to a Fourier series, by exchanging the order of summations and exploiting (7),

$$S(r,\alpha,\beta,\omega) = \sum_{m=-\infty}^{\infty} e^{im\alpha}\times \times \sum_{n=|m|}^{\infty} \breve{S}_n^m(\omega)j_n\big(\tfrac{\omega}{c}r\big)Y_n^m(\beta,0). \quad (11)$$

If we compare (1) with (11) in a horizontal plane, $z = r\cos\beta$,

$$\mathring{S}_m(\omega)J_m\big(\tfrac{\omega}{c}r\sin\beta\big) = \sum_{n=|m|}^{\infty} \breve{S}_n^m(\omega)j_n\big(\tfrac{\omega}{c}r\big)Y_n^m(\beta,0), \quad (12)$$

where the variables of the cylindrical coordinate system were replaced, $\rho = r\sin\beta, \phi = \alpha$. By using the

expansion coefficients of plane waves, (2) and (9), the Bessel function of the first kind is represented as a weighted sum of spherical Bessel functions of the first kind,

$$i^{-m} J_m\big(\tfrac{\omega}{c} r \sin\beta\big) = \\ = \sum_{n=|m|}^{\infty} 4\pi i^{-n} Y_n^m(\tfrac{\pi}{2}, 0)^* Y_n^m(\beta, 0) j_n\big(\tfrac{\omega}{c} r\big) \quad (13)$$

where the phase term $e^{-im\alpha_{\mathrm{pw}}}$ is canceled out. Finally, by substituting $J_m\big(\frac{\omega}{c} r \sin\beta\big)$ in (12) with (13), the relation of the expansion coefficients in spherical and circular harmonics representations are obtained,

$$\breve{S}_n^m(\omega) = 4\pi i^{m-n} Y_n^m(\tfrac{\pi}{2}, 0)^* \mathring{S}_m(\omega). \quad (14)$$

For instance, a monopole line source is represented by spherical harmonics with the coefficients of

$$\breve{S}_{n,\mathrm{ls}}^m(\omega) = -\pi i^{m-n+1} H_m^{(2)}\big(\tfrac{\omega}{c} r_{\mathrm{ls}}\big) Y_n^m(\tfrac{\pi}{2}, \alpha_{\mathrm{ls}})^*. \quad (15)$$

The position of a line source is defined by its position in the xy-plane. The circular harmonics expansion coefficients of monopole or higher-order line source, can now be converted into spherical harmonics coefficients.

The conversion between these two representations was also presented, e.g., in [10, Eq. (13)] and [11, Eq. (3.47)] in the context of sound field analysis, and also in [12, Appendix] using a different derivation.

3. NFC-HOA

In NFC-HOA, the sound field reproduced by secondary monopole sources continuously distributed on the surface of a sphere with a radius of r_0 is given as

$$\hat{S}(r, \alpha, \beta, \omega) = \\ = \int_0^{2\pi} \int_0^{\pi} D(\mathbf{x}_0, \omega) G(\mathbf{x}|\mathbf{x}_0, \omega) r_0^2 \sin\beta \mathrm{d}\alpha \mathrm{d}\beta \quad (16)$$

where $\mathbf{x}_0 = (r_0, \alpha_0, \beta_0)$ is the position of a secondary source on the boundary surface, $D(\mathbf{x}_0, \omega)$ the corresponding driving function, and $r_0^2 \sin\beta \mathrm{d}\alpha \mathrm{d}\beta$ the surface element. The Green's function $G(\mathbf{x}|\mathbf{x}_0, \omega)$ characterizes the acoustic transmission from a secondary source $\mathbf{x}_0$ to a field point $\mathbf{x} \neq \mathbf{x}_0$. Equation (16) is solved with respect to the driving function $D(\mathbf{x}_0, \omega)$, such that the reproduced sound field in V equals the desired one $\hat{S}(\mathbf{x}, \omega) = S(\mathbf{x}, \omega)$. NFC-HOA is based on the explicit solution of (16). Due to the spherical symmetry of the problem, each term in (16) is expanded into spherical harmonics. The driving function is given by comparing the individual expansion coefficients. In this paper, the detailed derivation is omitted and the results from earlier studies are adopted. Theoretical details of NFC-HOA are presented in [13], and comparison with other methods can be found in [14, 15].

3.1. Secondary Point Sources

A spherical distribution of secondary point sources can perfectly reconstruct 3D sound fields, and a circular distribution of secondary line sources can achieve perfect reconstruction of 2D sound fields. The latter, however, is not feasible as a line source cannot be realized. In so-called 2.5D synthesis, the line sources are replaced by point sources, which results in dimensionality mismatch between the sound field and the secondary sources.

In practical sound field synthesis systems, loudspeakers mounted in closed enclosures are employed, which reasonably approximates monopole sources up to moderate frequencies. If we assume free-field propagation and ignore the interaction between the secondary sources, $G(\mathbf{x}|\mathbf{x}_0, \omega)$ is given as the 3D free-field Green's function and its spherical harmonics expansion coefficient as

$$\breve{G}_n^m(\omega) = -i\tfrac{\omega}{c} h_n^{(2)}\big(\tfrac{\omega}{c} r_0\big) Y_n^m(0, 0)^*, \quad (17)$$

which is evaluated for the secondary source at $\mathbf{x}_0 = (r_0, 0, 0)$.

3.2. 3D Driving Functions

Note that Eq. (16) constitutes a spherical convolution of the driving function and the 3D Green's function, which is equivalent to the multiplication of the corresponding spherical harmonics expansion coefficient. Thus, the coefficient of the driving function is given as [13]

$$D_{3\mathrm{D}}(\alpha_0, \beta_0, \omega) = \\ \frac{1}{2\pi r_0^2} \sum_{n=0}^{\infty} \sum_{m=-n}^{n} \sqrt{\frac{2n+1}{4\pi}} \frac{\breve{S}_n^m(\omega)}{\breve{G}_n^0(\omega)} Y_n^m(\beta_0, \alpha_0). \quad (18)$$

The mode of $\breve{G}_n^m(\omega)$ is set to $m = 0$ due to the property of spherical convolution [16, p. 210]. Note

that, for certain frequencies, the driving function has a non-uniqueness problem due to the zeros of the denominator. But it was shown that this can be overcome and (18) is still a valid solution [17, 18]. This is also to case for the 2.5D NFC-HOA driving function introduced in the following subsection. To obtain the 3D NFC-HOA driving function of a 2D sound field, (14) and (17) is plugged into (18),

$$D_{\mathrm{3D}}(\alpha_0,\beta_0,\omega) = \frac{2}{r_0^2}\sum_{n=0}^{\infty}\sum_{m=-n}^{n}\frac{i^{n-m+1}\mathring{S}_m(\omega)}{\frac{\omega}{c}h_n^{(2)}\left(\frac{\omega}{c}r_0\right)}\times \\ \times Y_n^m(\tfrac{\pi}{2},0)^* Y_n^m(\beta_0,\alpha_0). \quad (19)$$

The driving function of a monopole line source at $(r_{\mathrm{ls}},\alpha_{\mathrm{ls}},0)$ is obtained by using the coefficient from Table 1,

$$D_{\mathrm{3D,ls}}(\alpha_0,\beta_0,\omega) = \frac{1}{2r_0^2}\sum_{n=0}^{\infty}\sum_{m=-n}^{n}\frac{i^{n-m}H_m^{(2)}\left(\frac{\omega}{c}r_{\mathrm{ls}}\right)}{\frac{\omega}{c}h_n^{(2)}\left(\frac{\omega}{c}r_0\right)}\times \\ \times Y_n^m(\tfrac{\pi}{2},\alpha_{\mathrm{ls}})^* Y_n^m(\beta_0,\alpha_0). \quad (20)$$

3.3. 2.5D Driving Functions

In 2.5D synthesis, Eq. (16) degenerates to a contour integral on a circle, thus constituting a circular convolution. Analogous to the 3D case, the driving function is given in terms of circular harmonics [13],

$$D_{\mathrm{2.5D}}(\alpha_0,\omega) = \frac{1}{2\pi r_0}\sum_{m=-\infty}^{\infty}\frac{\breve{S}_{|m|}^m(\omega)}{\breve{G}_{|m|}^m(\omega)}e^{im\alpha_0}. \quad (21)$$

In the derivation, although not obvious from (21), a reference radius of $r=0$ is chosen so that the radial dependency of the driving function is removed. As a result, the reproduced sound field is correct only at the central position, and amplitude errors are introduced elsewhere. This is a typical property of 2.5D sound field synthesis. Again, the driving function of a general 2D sound field is obtained by substituting (12) and (17) into (21),

$$D_{\mathrm{2.5D}}(\alpha_0,\omega) = \\ = \frac{2}{r_0}\sum_{m=-\infty}^{\infty}\frac{i^{m-|m|+1}\mathring{S}_m(\omega)}{\frac{\omega}{c}h_{|m|}^{(2)}\left(\frac{\omega}{c}r_0\right)}e^{im\alpha_0}. \quad (22)$$

The driving function of a virtual line source at $(r_{\mathrm{ls}},\alpha_{\mathrm{ls}},0)$ is thus,

$$D_{\mathrm{2.5D,ls}}(\alpha_0,\omega) = \\ = \frac{1}{2r_0}\sum_{m=-\infty}^{\infty}\frac{i^{m-|m|}H_m^{(2)}\left(\frac{\omega}{c}r_{\mathrm{ls}}\right)}{\frac{\omega}{c}h_{|m|}^{(2)}\left(\frac{\omega}{c}r_0\right)}e^{im(\alpha_0-\alpha_{\mathrm{ls}})}. \quad (23)$$

4. RESULTS

In this section, numerical simulations of the synthesized sound fields are presented. The driving function (20) or (23) are used to drive ideal secondary point sources, and the reproduced sound fields are computed using a discretized version of (16). In 3D sound field synthesis, a spherical array consisting of $N_{\mathrm{3D}} = 484$ secondary sources is used, whereas in 2.5D cases, a circular array with $N_{\mathrm{2.5D}} = 64$ secondary sources is used. Both arrays have the same radius of $r_0 = 1.5$ m. The secondary sources of the circular array have an equiangular distribution. The secondary source distribution of the spherical array was computed by using the *Riesz s-energy approach* [19]. The upper bounds of the summations in (20) and (23) were truncated to finite numbers

$$M_{\mathrm{3D}} = \sqrt{N_{\mathrm{3D}}} - 1 = 21$$
$$M_{\mathrm{2.5D}} = N_{\mathrm{2.5D}}/2 - 1 = 31,$$

thus the spatial bandwidth of the driving functions is band-limited. Due to spatial sampling and spatial bandwidth limitation, reconstruction errors are introduced in the synthesized sound fields, mostly concentrated above an upper bound frequency given as [20]

$$f = \frac{Mc}{2\pi r_0}. \quad (24)$$

This corresponds to

$$f_{\mathrm{3D}} \approx 764.3 \text{ Hz} \quad (25)$$
$$f_{\mathrm{2.5D}} \approx 1128.2 \text{ Hz}, \quad (26)$$

in 3D and 2.5D synthesis, respectively ($c = 343$ m/s). Note that, the reconstruction errors are also position dependent. The synthesized sound field has a nearly-artifact-free region around the center of the array, whereas the sound field outside it suffers from deviations. The size of this region is given as [6, (2.41)]

$$r_M = \frac{Mc}{2\pi f}. \quad (27)$$

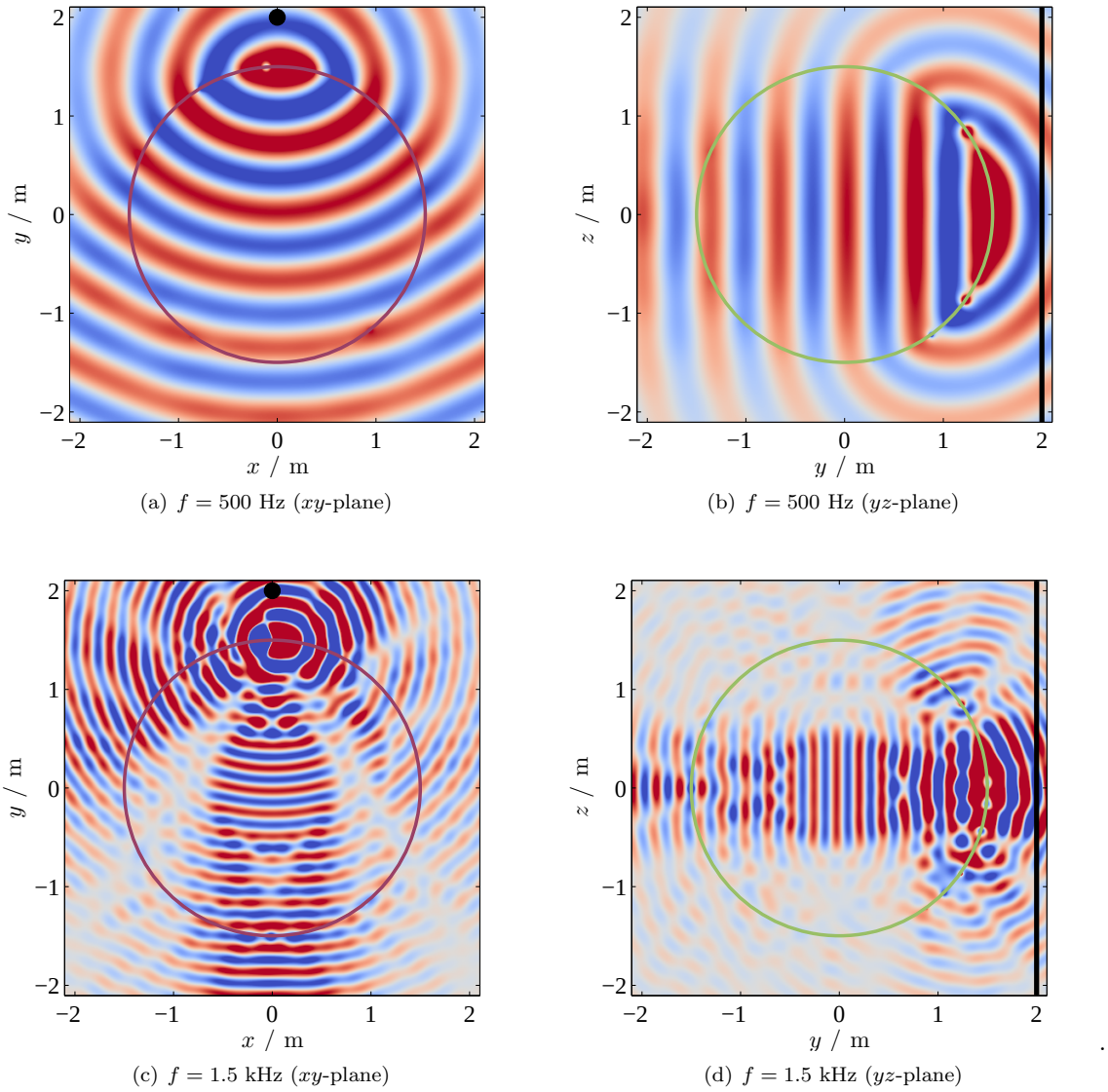

(a) $f = 500$ Hz (xy-plane)

(b) $f = 500$ Hz (yz-plane)

(c) $f = 1.5$ kHz (xy-plane)

(d) $f = 1.5$ kHz (yz-plane)

Fig. 1: Synthesized sound fields, $\Re\{\hat{S}(\mathbf{x}, \omega)\}$, of a virtual line source ($r_{\text{ls}} = 2$ m, $\alpha_{\text{ls}} = \frac{\pi}{2}$ rad) using 3D NFC-HOA ($N = 484$, $r_0 = 1.5$ m). For better visibility, the secondary sources are not shown, and the boundary of the array is indicated by circles instead (◯ in the xy-plane and ◯ in the yz-plane). The virtual source is indicated by a black circle • in the xy-plane (top view), and by thick black lines in the yz-plane (side view).

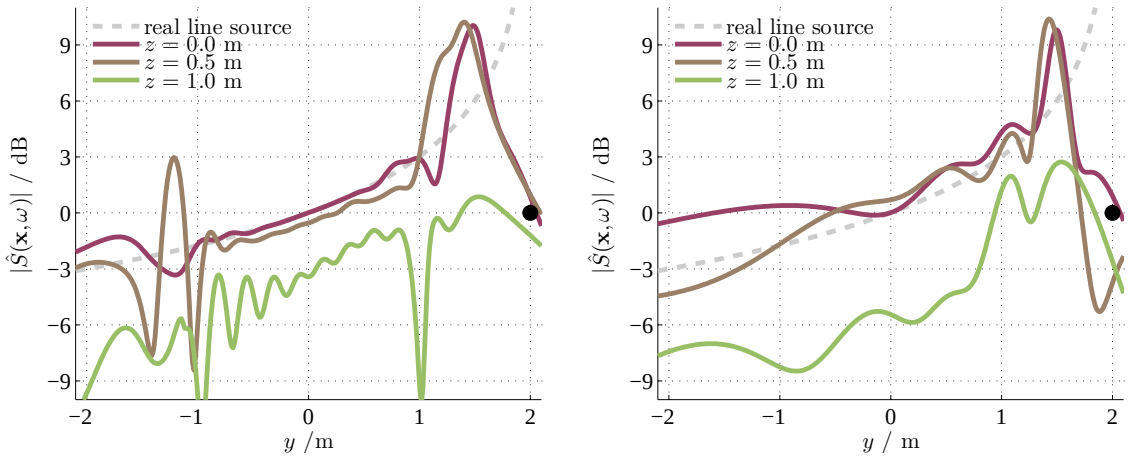

(a) NFC-HOA (b) WFS

Fig. 2: Amplitude decay in the synthesized sound field of a virtual line source ($r_{\mathrm{ls}} = 2$ m, $\alpha_{\mathrm{ls}} = \frac{\pi}{2}$ rad, $f = 750$ Hz) synthesized by 3D sound field synthesis ($N = 484$, $r_0 = 1.5$ m). The position of the virtual line source is indicated by the black circle •, and the amplitude decay of a real line source by the dashed gray line. The results were normalized such that the sound field at $\mathbf{x} = \mathbf{0}$ is 0 dB.

The focus of our observation is on the amplitude decay in the synthesized sound field. The sound field of an ideal line source has constant amplitude along the longitudinal direction, while exhibits a 3 dB attenuation per doubled distance along its radial direction. As noted before, the geometrical attenuation of a virtual source in 2.5D sound field synthesis suffers from deviations. Moreover, the amplitude decay shows different behavior depending on whether the listener is moving in the listening area or the source is moving in the virtual space [6, Sec. 5.3.4].

The influence of the limited number of secondary sources on the synthesized sound field are not treated in detail. For a comprehensive analysis of spatial sampling and spatial bandwidth limitation, the reader is referred to [21, 22].

The numerical simulations are based on the Sound Field Synthesis Toolbox [23]. Although the NFC-HOA driving functions of virtual line sources are not implemented in the current released verion (1.0.1), the scripts used for the simulations are available for download at `http://spatialaudio.net/virtual-cylindrical-waves`.

4.1. 3D NFC-HOA

Figure 1(a) and 1(b) are the cross-sections of the sound fields of a virtual line source with a frequency of $f = 500$ Hz and positioned at $(2, \frac{\pi}{2}, 0)$. The desired sound field is correctly synthesized within the listening area, apart from a slight amplitude deviation observed on the yz-plane. In the case of a virtual line source with a frequency $f = 1.5$ kHz, higher than the frequency in (25), the performance is degraded as shown in Fig. 1(c) and 1(d). The desired sound field is only observed around the center of the spherical array. The existence of such error-free region is a well-known property of NFC-HOA [21]. For a given configuration and allowable error criterion, the radius of the region is inversely proportional to the frequency.

In Fig. 2(a), the amplitude at different heights are shown for a virtual line source ($f = 750$ Hz). In the range of $|y| < 1$, the amplitude is almost perfect at $z = 0$, and only slightly deviated at $z = 0.5$. Outside this range, strong deviation and fluctuation occur. Fig. 2(b) shows the amplitude decay of the same virtual line source synthesized using WFS. The amplitude is very high in the vicinity of the virtual source, and decreases more or less monotonically with a slight fluctuation. There is no apparent error-free region.

In Fig. 3, virtual line source emits four different frequencies, from 250 Hz to 2 kHz with an interval of one octave. In Fig. 3(a), the error-free region in NFC-HOA gets smaller for higher frequencies. The amplitude drops off exactly 3 dB per octaves. This is due to the low-pass characteristic of line sources. WFS, shown in Fig. 3(b), suffers from amplitude error in the entire listening area, even for frequencies below the spatial aliasing frequency. Each amplitude asymptotically converges to the desired amplitude with an offset of 3 dB. In terms of spectral balance, better performance is expected for NFC-HOA at the center of the array, but strong spectral variation is likely to occur even with a slight movement, as presented in [24]. The spectral variation in WFS is relatively gradual.

So far, the source was fixed and the amplitude distribution within the listening area was examined. Fig. 4 shows the amplitude at the center of the listening area, while moving the source along the y-axis. Only non-focused sources ($r_{\mathrm{ls}} > r_0$) were considered. For distance lager than 4 m, the amplitude agrees with the -3 dB decay per doubled-distance rule. While the amplitude in NFC-HOA smoothly decays, deviations occur in WFS, especially near the secondary sources. This is due to the WFS driving function which grows inversely proportional to the distance between the virtual source and the secondary source [2].

4.2. 2.5D NFC-HOA

The same scenarios were considered for 2.5D synthesis. The sound field of a line source ($f = 750$ Hz) at $\mathbf{x}_{\mathrm{ls}} = (2, \frac{\pi}{2}, 0)$ is shown in Fig. 5(a). Above the frequency in (26), in Fig. 5(b), the synthesized sound field is contaminated by reconstruction errors. Within the error-free region, only the phase of the desired sound fields is correctly synthesized.

In Fig. 6, a number of virtual source models are compared in terms of amplitude decay within the listening area, along the y-axis. Not surprisingly, the virtual line source and virtual point source exhibit the same decay of -6 dB per doubled distance, both in NFC-HOA and WFS. This seems to be an inherent characteristic in 2.5D sound field synthesis which is unavoidable.

Fig. 7 shows the frequency dependency of the amplitude decay in the listening area, which is always steeper than in theory. The low pass characteristic (-3 dB/octave) is preserved in NFC-HOA within the error-free region, which is not the case in WFS. The large amplitudes at $y_0 = -1.5$ m in Fig. 7(a) are due to the fact that NFC-HOA always activates every secondary sources. WFS, on the other hand, uses only the secondary sources that are illuminated by the virtual source [25].

The amplitude changes due the source position are shown in Fig. 8. In NFC-HOA, each virtual source model exhibits the desired decay rate, whereas in WFS, the virtual point source and line source have almost the same amplitude behavior.

4.3. Further Discussions

The sound field emitted by a line source exhibits a low-pass characteristic, as can be noted from the properties of the Hankel function [9, Ch. 9]. To employ a virtual line source in sound field synthesis, it might be favorable to equalize its spectrum. This can be done, by applying an equalization filter with a slope of $+3$ dB/octave to the driving function, e.g., filtering by $\sqrt{i\frac{\omega}{c}}$.

The spherical Hankel function appearing in the denominator in (20) and (23) can be realized by recursive filters [26, 27], thereby enabling an real-time implementation [28]. For the Hankel function in the numerator, however, such an efficient implementation is not known so far. Thus, the driving functions have to be computed by using traditional filter design methods, e.g., bilinear transform [29, Sec. 16.2.3.2].

5. CONCLUSIONS

The driving function of virtual cylindrical waves, (20) and (23), were derived both in 3D and 2.5D NFC-HOA. This is done by converting the circular harmonics expansion coefficients to spherical harmonics expansion coefficients. The properties of the reproduced sound fields were investigated through numerical simulations, with our focus on the amplitude distribution within the listening area, as well as on the amplitude change due to the source movement in the virtual space. Comparing the results with WFS reveal that NFC-HOA is somewhat superior in terms of amplitude accuracy, especially near the center of the listening area.

The observations on the physical properties of synthetic sound fields, presented in this paper, might

be associated with loudness perception or auditory distance perception of virtual sound source [30, 31]. However, no concrete conclusion can be drawn at this stage, as the latter are still open topics even for real sound sources [32, 33].

6. REFERENCES

[1] A. J. Berkhout, D. de Vries, and P. Vogel, "Acoustic control by wave field synthesis," *The Journal of the Acoustical Society of America*, vol. 93, no. 5, pp. 2764–2778, 1993.

[2] S. Spors, R. Rabenstein, and J. Ahrens, "The theory of wave field synthesis revisited," in *124th AES Convention*, pp. 17–20, 2008.

[3] J. Daniel, S. Moreau, and R. Nicol, "Further investigations of high-order ambisonics and wavefield synthesis for holophonic sound imaging," in *Audio Engineering Society Convention 114*, 2003.

[4] J. Ahrens and S. Spors, "Applying the ambisonics approach to planar and linear distributions of secondary sources and combinations thereof," *Acta Acustica united with Acustica*, vol. 98, no. 1, pp. 28–36, 2012.

[5] H. Wierstorf, *Perceptual Assessment of Sound Field Synthesis*. PhD thesis, Technische Universität Berlin, 2014.

[6] J. Ahrens, *Analytic Methods of Sound Field Synthesis*. Springer, 2012.

[7] H. Teutsch, *Modal Array Signal Rrocessing: Principles and Applications of Acoustic Wavefield Decomposition*, vol. 348. Springer, 2007.

[8] E. G. Williams, *Fourier Acoustics: Sound Radiation and Nearfield Acoustical Holography*. academic press, 1999.

[9] M. Abramowitz and I. A. Stegun, *Handbook of Mathematical Functions: with Formulas, Graphs, and Mathematical Tables*. No. 55, Courier Dover Publications, 1972.

[10] M. R. Thomas, J. Ahrens, and I. J. Tashev, "A method for converting between cylindrical and spherical harmonic representations of sound fields," in *IEEE International Conference on Acoustics, Speech, and Signal Processing (ICASSP)*, 2011.

[11] A. Kuntz, *Wave Field Analysis Using Virtual Circular Microphone Arrays*. Verlag Dr. Hut, 2008.

[12] D. B. Ward and T. D. Abhayapala, "Reproduction of a plane-wave sound field using an array of loudspeakers," *Speech and Audio Processing, IEEE Transactions on*, vol. 9, no. 6, pp. 697–707, 2001.

[13] J. Ahrens and S. Spors, "An analytical approach to sound field reproduction using circular and spherical loudspeaker distributions," *Acta Acustica united with Acustica*, vol. 94, pp. 988–999, Nov. 2008.

[14] F. Fazi, P. A. Nelson, and R. Potthast, "Analogies and differences between three methods for sound field reproduction," in *Ambisonics Symposium*, 2009.

[15] F. Schultz and S. Spors, "Comparing Approaches to the Spherical and Planar Single Layer Potentials for Interior Sound Field Synthesis," *Acta Acustica united with Acustica*, vol. 100, pp. 900–911, 2014.

[16] J. R. Driscoll and D. M. Healy, "Computing fourier transforms and convolutions on the 2-sphere," *Advances in applied mathematics*, vol. 15, no. 2, pp. 202–250, 1994.

[17] F. M. Fazi and P. A. Nelson, "Nonuniqueness of the solution of the sound field reproduction problem with boundary pressure control," *Acta Acustica united with Acustica*, vol. 98, no. 1, pp. 1–14, 2012.

[18] F. Zotter and S. Spors, "Is sound field control determined at all frequencies? How is it related to numerical acoustics?," in *Audio Engineering Society Conference: 52nd International Conference: Sound Field Control-Engineering and Perception*, Audio Engineering Society, 2013.

[19] E. B. Saff and A. B. Kuijlaars, "Distributing many points on a sphere," *The mathematical intelligencer*, vol. 19, no. 1, pp. 5–11, 1997.

[20] R. A. Kennedy, P. Sadeghi, T. D. Abhayapala, and H. M. Jones, "Intrinsic limits of dimensionality and richness in random multipath fields," *Signal Processing, IEEE Transactions on*, vol. 55, no. 6, pp. 2542–2556, 2007.

[21] S. Spors and J. Ahrens, "A comparison of wave field synthesis and higher-order ambisonics with respect to physical properties and spatial sampling," in *Audio Engineering Society Convention 125*, 2008.

[22] J. Ahrens, S. Spors, and H. Wierstorf, "Comparison of higher order ambisonics and wave field synthesis with respect to spatial discretization artifacts in time domain," in *Audio Engineering Society Conference: 40th International Conference: Spatial Audio: Sense the Sound of Space*, 2010.

[23] H. Wierstorf and S. Spors, "Sound field synthesis toolbox," in *Audio Engineering Society Convention 132*, 2012.

[24] J. Ahrens and S. Spors, "Alterations of the temporal spectrum in high-resolution sound field reproduction of different spatial bandwidths," in *Audio Engineering Society Convention 126*, 2009.

[25] S. Spors, "Extension of an analytic secondary source selection criterion for wave field synthesis," in *Audio Engineering Society Convention 123*, 2007.

[26] S. Spors, V. Kuscher, and J. Ahrens, "Efficient realization of model-based rendering for 2.5-dimensional near-field compensated higher order ambisonics," in *Applications of Signal Processing to Audio and Acoustics (WASPAA), 2011 IEEE Workshop on*, pp. 61–64, 2011.

[27] H. Pomberger and D. F. Zotter, *Angular and Radial Directivity Control for Spherical Loudspeaker Arrays*. University of Music and Dramatic Arts, Graz, 2008.

[28] M. Geier, J. Ahrens, and S. Spors, "The SoundScape Renderer: A Unified Spatial Audio Reproduction Framework for Arbitrary Rendering Methods," in *Audio Enginerring Society Convention 124*, 2008.

[29] B. Girod, R. Rabenstein, and A. Stenger, *Signals and Systems*. Wiley New York, 2001.

[30] F. Völk, M. Straubinger, and H. Fastl, "Psychoacoustical experiments on loudness perception in wave field synthesis," in *20th Int. Congress on Acoustics (ICA)*, 2010.

[31] F. Völk, "Psychoakustische experimente zur distanz mittels wellenfeldsynthese erzeugter hörereignisse," in *Tagungsband Fortschritte der Akustik, DAGA 2010*, pp. 1065–1066, 2010.

[32] J. Blauert, *Spatial Hearing: the Psychophysics of Human Sound localization*. MIT press, 1997.

[33] P. Zahorik, D. S. Brungart, and A. W. Bronkhorst, "Auditory distance perception in humans: A summary of past and present research," *Acta Acustica united with Acustica*, vol. 91, no. 3, pp. 409–420, 2005.

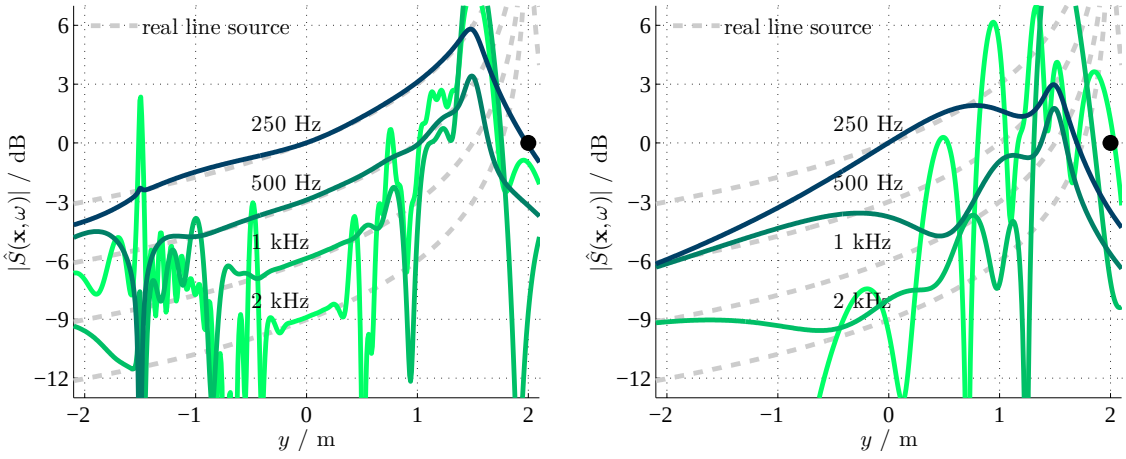

(a) NFC-HOA (b) WFS

Fig. 3: Amplitude decay in the synthesized sound field of a virtual line source ($r_{\text{ls}} = 2$ m, $\alpha_{\text{ls}} = \frac{\pi}{2}$ rad) synthesized by 3D sound field synthesis ($N = 484$, $r_0 = 1.5$ m). The virtual line source is indicated by the black circle •, and the amplitude decay of a real line sources by dashed gray lines. The sound field of $f = 250$ Hz was normalized to 0 dB at $y = 0$.

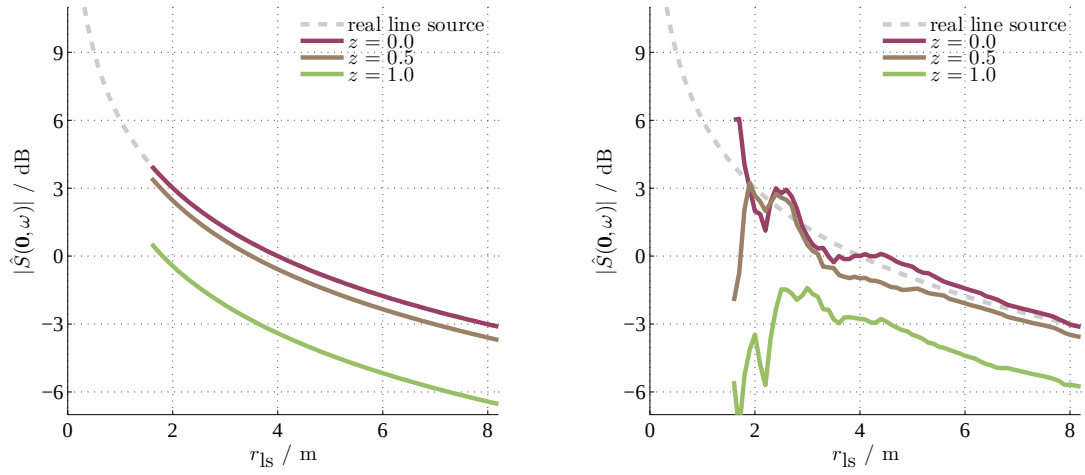

(a) NFC-HOA (b) WFS

Fig. 4: Sound field at the origin synthesized using 3D sound field synthesis ($N = 484$, $r_0 = 1.5$ m). Monochromatic virtual line source ($\alpha_{\text{ls}} = \frac{\pi}{2}$ rad, $f = 750$ Hz) moved on the y-axis. The dashed gray line indicates the amplitude of a real line source.

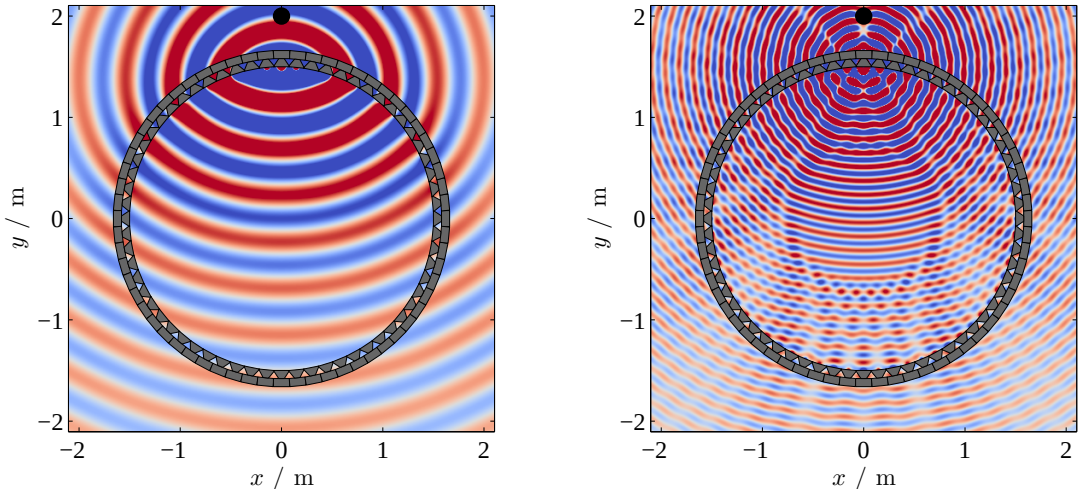

(a) $f = 750$ Hz (b) $f = 2.5$ kHz

Fig. 5: Synthesized sound fields, $\Re\{\hat{S}(\mathbf{x}, \omega)\}$, of a virtual line source ($r_{\text{ls}} = 2$ m, $\alpha_{\text{ls}} = \frac{\pi}{2}$ rad) using 2.5D NFC-HOA ($N = 64$, $r_0 = 1.5$ m). The virtual line source is denoted by black circles •.

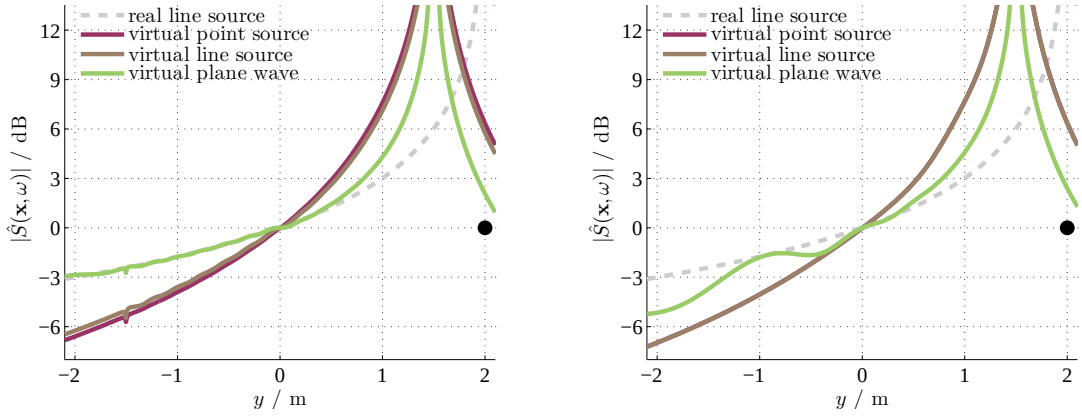

(a) NFC-HOA (b) WFS

Fig. 6: Amplitude decay in the synthesized sound field of a virtual line source ($r_{\text{ls}} = 2$ m, $\alpha_{\text{ls}} = \frac{\pi}{2}$ rad, $f = 750$ Hz) synthesized by 2.5D sound field synthesis ($N = 64$, $r_0 = 1.5$ m). The position of the virtual line source is indicated by the black circle •, and the amplitude decay of a real line source by the dashed gray line. The sound fields are normalized to 0 dB at $y = 0$.

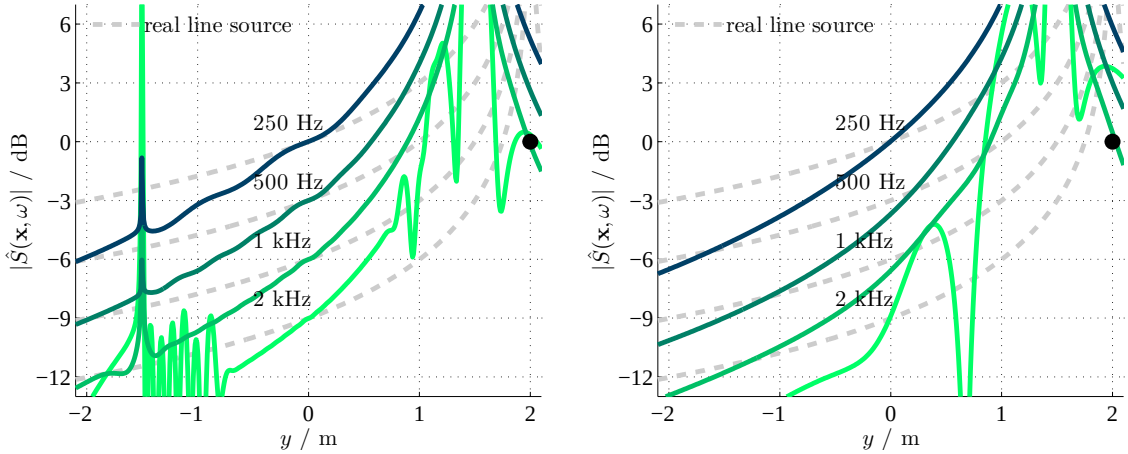

(a) NFC-HOA (b) WFS

Fig. 7: Amplitude decay in the sound field of a virtual line source ($r_{\text{ls}} = 2$ m, $\alpha_{\text{ls}} = \frac{\pi}{2}$ rad) synthesized by 2.5D sound field synthesis ($N = 64$, $r_0 = 1.5$ m). The virtual line source is indicated by the black circle •, and the amplitude decay of a real line sources by dashed gray lines. The sound field of $f = 250$ Hz was normalized to 0 dB at $y = 0$.

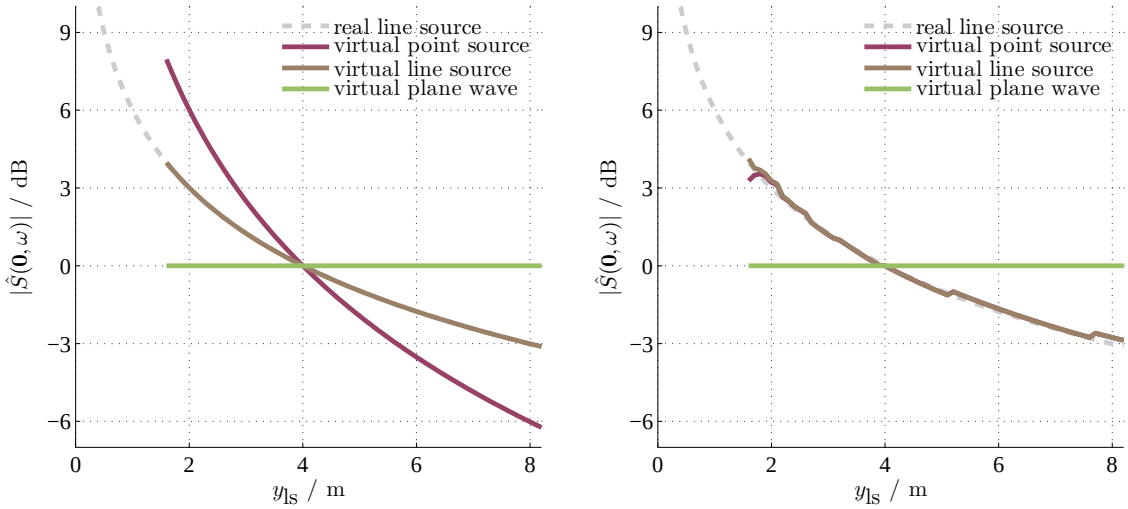

(a) NFC-HOA (b) WFS

Fig. 8: Sound field at the origin synthesized using 2.5D sound field synthesis ($N = 64$, $r_0 = 1.5$ m). Monochromatic virtual line source ($\alpha_{\text{ls}} = \frac{\pi}{2}$ rad, $f = 750$ Hz) moved on the y-axis. The dashed gray line indicates the amplitude of a real line source.